

Symmetry-reduced model reduction of shift-equivariant systems via operator inference

Yu Shuai^{1*} and Clarence W. Rowley¹

^{1*}Department of Mechanical and Aerospace Engineering, Princeton University, Princeton, 08540, New Jersey, United States.

*Corresponding author(s). E-mail(s): yu_shuai@princeton.edu;
Contributing authors: cwrowley@princeton.edu;

Abstract

We consider data-driven reduced-order models of partial differential equations with shift equivariance. Shift-equivariant systems typically admit traveling solutions, and the main idea of our approach is to represent the solution in a traveling reference frame, in which it can be described by a relatively small number of basis functions. Existing methods for operator inference allow one to approximate a reduced-order model directly from data, without knowledge of the full-order dynamics. Our method adds additional terms to ensure that the reduced-order model not only approximates the spatially frozen profile of the solution, but also estimates the traveling speed as a function of that profile. We validate our approach using the Kuramoto-Sivashinsky equation, a one-dimensional partial differential equation that exhibits traveling solutions and spatiotemporal chaos. Results indicate that our method robustly captures traveling solutions, and exhibits improved numerical stability over the standard operator inference approach.

Keywords: Shift equivariance, symmetry reduction, reduced-order models, operator inference

MSC Classification (2010): 35B06 , 35Q35 , 47A58 , 65D15 , 68W25

1 Introduction

Spatially extended systems governed by partial differential equations (PDEs) are central to many areas of physical science, including fluid dynamics, chemical reactions,

and atmospheric science. These PDEs typically describe spatiotemporal scalar, vector, or tensor fields and often exhibit discrete or continuous symmetries such as translation, rotation, or reflection invariance. In particular, shift-equivariant PDEs, which are invariant under spatial translations, allow solutions to drift continuously in space while preserving their temporal evolution. This symmetry typically implies that the PDE lacks explicit dependence on spatial coordinates. In fluid mechanics, for instance, channel flows or circular pipe flows governed by the Navier-Stokes equations possess shift equivariance with periodic boundary conditions in streamwise and spanwise (azimuthal) directions. In such systems, propagating coherent structures such as traveling waves, relative periodic orbits and localized turbulent patches have been identified and shown to play central roles in turbulent dynamics [1–6]. Despite their low-dimensional dynamics, resolving these structures in direct numerical simulations still requires finely resolved spatial grids [1, 2]. This motivates the development of reduced-order models (ROMs) that exploit the intrinsic low-rank behavior of such systems, providing efficient and interpretable surrogates for full-order models (FOMs).

To construct ROMs for shift-equivariant systems, a common approach is the (Petrov-)Galerkin projection onto spatial modes obtained via proper orthogonal decomposition (POD) [7, 8]. However, for traveling solutions, the optimal POD modes that preserve the symmetry are Fourier modes [7], which offer limited additional insight, especially when the underlying PDEs are already simulated using spectral methods. Moreover, many Fourier modes are typically required to accurately represent propagating solutions, even if the shape of the traveling solution remains relatively constant. This inefficiency stems from POD’s assumption that spatiotemporal data can be separated into spatial modes and temporal coefficients, which fails for solutions with spatial drift over time. Consequently, the solution manifold has a large Kolmogorov n -width, meaning that the projection error onto a n -dimensional linear subspace decays slowly [9]. To address this, various methods have been developed to better capture the transport nature of these systems. Template fitting [10], also called the method of slices [3, 11–13], removes spatial drift by aligning solution snapshots against a “template,” converting propagating structures into stationary profiles. These aligned profiles can then be accurately represented with fewer POD modes. This idea has been widely used in studying exact coherent structures in fluid flows, and forms the basis of the symmetry-reduced Galerkin ROM (SR-Galerkin ROM), where the dynamics of the non-drifting profiles are modeled in low dimensions and the original solution is recovered via a reconstruction equation that tracks the spatial displacement in real time. Other approaches aim to directly model the traveling solutions using adaptive basis functions. The shifted POD (sPOD) algorithm [14], for example, represents the solution using snapshot-wise shifted POD modes with optimized shifting amount. Similarly, the method of unsupervised traveling wave identification with shifting and truncation (UnTWIST) [15] learns the shifting amount as a time-dependent function from a predefined library during training. While these methods effectively extract low-rank structure, they are limited to analysis of the training data and do not generalize easily for predictive modeling of new solutions, since the shifting information is not dynamically inferred in the forecast stage. To overcome this drawback, an online model reduction framework was proposed in [16], where the POD basis is

adaptively updated during time integration via low-rank corrections. This allows the ROM to dynamically track solution evolution without relying on precomputed shifts, enabling better generalization to unseen states.

The aforementioned ROMs based on symmetry reduction and online adaptive bases are all built upon Galerkin projection. As such, they are *intrusive* methods requiring explicit knowledge of the full-order equations, i.e., full-order models (FOM), to perform dimension reduction. To extend model reduction to settings where the FOM is inaccessible or treated as a black box, *non-intrusive* data-driven approaches, such as dynamic mode decomposition (DMD) [17–19] and operator inference (OpInf) [20–22], offer promising alternatives by relying solely on solution snapshots and their time derivatives. In the DMD framework, the physics-informed DMD (piDMD) method [23] enforces commutativity between the learned linear operator and the spatial shift operator to preserve shift equivariance in the reduced model. However, this constraint restricts the DMD modes to Fourier modes, which often fail to capture the coherent structures in the data efficiently. To avoid the reliance on Fourier modes, other methods perform dimension reduction on the non-traveling solution profiles. The characteristic DMD algorithm [24] eliminates drift by rotating the space-time frame under the assumption of constant group velocity. More recently, symmetry-reduced DMD (SRDMD, [25, 26]) uses template-fitted snapshots as input and constructs a best-fit linear model for the stationary profiles to reveal the low-rank dynamics of coherent structures and to facilitate the identification of unstable periodic orbits embedded in transitional and turbulent flows. Operator Inference can also be combined with UnTWIST to create shifted OpInf ROMs [27], where the shifting amount is learned offline as an analytical function of time, and the reduced model is built for the stationary profile using polynomial regression. Nevertheless, both symmetry-reduced DMD and shifted OpInf lack a mechanism for online prediction of shifting speed from reduced variables. Consequently, reconstructing the full drifting solutions from the frozen profiles remains an open challenge in these frameworks. More importantly, existing non-intrusive ROMs typically assume linear or low-order polynomial dynamics. In contrast, prior intrusive work such as the SR-Galerkin ROM [11] has revealed that the dynamics of symmetry-reduced systems consist of not only polynomial terms but also a rational symmetry-reduction term which captures the coupling between profile evolution and spatial propagation. This structure has yet to be fully replicated in non-intrusive ROMs and motivates the framework developed in this work.

In this work, we develop a non-intrusive ROM framework for shift-equivariant PDE systems by combining symmetry reduction techniques from [11], specifically the template fitting process and the reconstruction equation, with Operator Inference (OpInf). The resulting Symmetry-Reduced Operator Inference (SR-OpInf) ROM serves as a data-driven counterpart to the intrusive SR-Galerkin ROM, yet retains many of its advantages. Trained solely on solution data without any access to the full-order model (FOM), the SR-OpInf ROM approximates the dynamics of spatially aligned profiles using a compact set of non-Fourier POD modes. Crucially, our framework enables efficient real-time computation of the shifting amount via a reconstruction equation whose coefficients are learned from data. To our knowledge, this is the first non-intrusive ROM that allows the shifting speed to be inferred online from the reduced

variables—making it capable of accurately predicting both the direction and magnitude of spatial drift for previously unseen solutions. Moreover, by applying the re-projection technique [28] to pre-process the training snapshots, we show that the SR-OpInf operators can be learned through a convex optimization problem with a unique global optimum matching SR-Galerkin operators. This establishes a direct correspondence between the intrusive and non-intrusive frameworks and allows insights from the Galerkin formulation to be carried over. We demonstrate the effectiveness of our method on the Kuramoto–Sivashinsky equation (KSE), focusing on drifting wave solutions with beating temporal dynamics. Our evaluations confirm that the SR-OpInf ROM accurately reproduces the high-fidelity FOM simulation data in terms of the spatial profile of the solution, the reduced variable, and the shifting speed, while also preserving shift-equivariance under shifts in the initial condition. Moreover, with re-projected training data, the SR-OpInf ROM successfully replicates the forecasts of its intrusive counterpart, the SR-Galerkin ROM.

The remainder of the paper is organized as follows. Section 2 provides a brief overview of shift-equivariant systems and introduces several benchmark ROMs, including the standard Galerkin ROM, OpInf ROM, and the SR-Galerkin ROM. Section 3 presents the formulation and training algorithm of the proposed SR-OpInf ROM, and describes the re-projection technique as a pre-processing step that enables it to replicate the dynamics of an SR-Galerkin ROM derived via intrusive projection. In Section 4, we apply our method to the Kuramoto–Sivashinsky equation (KSE) and validate its performance in reconstructing both training and testing data. Finally, conclusions are drawn in Section 5.

2 Preliminaries

2.1 Shift-equivariant systems

We consider a one-dimensional¹ partial differential equation (PDE) governing the evolution of a scalar field $u(x, t)$ defined on the spatial domain $0 \leq x \leq L$ and time $t \geq 0$ with periodic boundary conditions $u(x + L, t) \equiv u(x, t)$:

$$\partial_t u = f(u), \quad (1)$$

where $\partial_t u$ denotes the partial derivative of $u(x, t)$ with respect to time t , and f is a (spatial) differential operator. We assume that the initial condition $u(x, 0)$ is sufficiently smooth for existence and uniqueness of solutions to this PDE, and we let \mathcal{U} denote the space of sufficiently smooth functions of x (i.e., for each t , $u(\cdot, t) \in \mathcal{U}$).

We now define the shift equivariance for system (1):

Definition 1 (Shift equivariance) Let S_θ denote the shift operator on functions in \mathcal{U} :

$$S_\theta[v](x) = v(x - \theta), \quad v \in \mathcal{U}. \quad (2)$$

¹For clarity of exposition, we present our methodology in the context of a one-dimensional shift-equivariant PDE. This setting captures the essential features of the problem while simplifying the notation. The proposed framework, however, generalizes naturally to higher-dimensional systems and can be applied to model reduction in those settings without conceptual modification.

The PDE (1) is shift equivariant if, for all $v \in \mathcal{U}$, $\theta \in \mathbb{R}$, we have

$$f(S_\theta[v]) \equiv S_\theta[f(v)]. \quad (3)$$

It follows immediately that, if f is shift equivariant, and $u(x, t)$ is a solution to the PDE (1), then any spatially shifted version $v_\theta(x, t) \equiv u(x - \theta, t)$, $\forall \theta \in \mathbb{R}$ is also a solution. This property leads naturally to the presence of traveling solutions that evolve over time while translating in space. A traveling solution $u(x, t)$ can be expressed in terms of its spatial profile $\hat{u}(x, t)$ as follows:

$$u(x, t) = \hat{u}(x - c(t), t), \quad (4)$$

where $c(t)$ is the shift amount. For instance, for the simple advection equation

$$\partial_t u + a \partial_x u = 0,$$

the corresponding $f(u) = -a \partial_x u$ is shift equivariant, and the equation admits traveling wave solutions of the form $u(x, t) = w(x - c(t))$, with $c(t) = at$. More generally, shift-equivariant systems can also support traveling solutions with time-varying profiles and shifting speeds.

2.2 Standard reduced-order models

We now give an overview of two standard model reduction techniques: the Galerkin method, and the Operator Inference method. Both approaches seek to approximate the full-state vector $u(t) \in \mathcal{U}$ using a low-dimensional basis, but they differ in how the reduced dynamics are obtained. In the Galerkin method, the dynamics are obtained through projection of the function f in (1) (which must be known), whereas in Operator Inference, the model is learned from data via regression.

Regarding notation, for the remainder of this paper, we regard the PDE (1) as a dynamical system evolving in the space \mathcal{U} , which consists of (periodic) functions of space x . Thus, at a particular time t , $u(t) \in \mathcal{U}$ is a function of space, equivalent to $u(\cdot, t)$.

2.2.1 Galerkin models for quadratic dynamics

To construct a Galerkin model, one usually begins by collecting an ensemble of snapshots $\{u(t_m)\}_{m=1}^{N_t}$ (each a function of space), which serves as the training dataset. One then typically subtracts the mean

$$\bar{u} = \frac{1}{N_t} \sum_{m=1}^{N_t} u(t_m), \quad (5)$$

and chooses n basis functions $\varphi_1, \dots, \varphi_n$ for a subspace of \mathcal{U} on which to project the equations. We will assume that \mathcal{U} is an inner product space, with the standard inner

product

$$\langle v, w \rangle = \frac{1}{L} \int_0^L v(x)w(x) dx, \quad v, w \in \mathcal{U}, \quad (6)$$

and that the basis functions are orthonormal (i.e., $\langle \varphi_i, \varphi_j \rangle = \delta_{ij}$). We then approximate $u(t)$ as

$$u(t) = \bar{u} + \sum_{i=1}^n a_i(t) \varphi_i, \quad (7)$$

where the coefficients $a_i(t) \in \mathbb{R}$ are the reduced variables.

A common choice for the basis is to perform proper orthogonal decomposition (POD) [7] on the set of mean-subtracted snapshots $\{u(t_1) - \bar{u}, \dots, u(t_{N_t}) - \bar{u}\}$. This is the procedure we shall use in the examples in Section 4, but the developments below are independent of the choice of basis; we assume only that the $\{\varphi_i\}$ are orthonormal.

For most of what follows, we will assume that the differential operator f in (1) is *quadratic*: that is, it has the form

$$f(u) = d + Au + B(u, u), \quad (8)$$

where $d \in \mathcal{U}$, $A : \mathcal{U} \rightarrow \mathcal{U}$ is linear, and $B : \mathcal{U} \times \mathcal{U} \rightarrow \mathcal{U}$ is bilinear (linear in each argument) and symmetric (i.e., $B(u, v) = B(v, u)$ for all $u, v \in \mathcal{U}$).

Galerkin projection then proceeds as follows. We would like to choose the coefficients $a_i(t)$ such that the expansion (7) satisfies the original PDE (1). However, this is in general not possible, as the true dynamics might drive $u(t)$ out of the subspace spanned by our n basis functions. So, in Galerkin projection, we simply project the dynamics (orthogonally) onto this subspace, and choose $a_i(t)$ so that

$$\langle \partial_t u, \varphi_i \rangle = \langle f(u), \varphi_i \rangle, \quad i = 1, \dots, n. \quad (9)$$

Using the fact that the basis functions φ_i are orthonormal, we obtain

$$\dot{a}_i = \langle d + Au + B(u, u), \varphi_i \rangle,$$

and inserting the expression (7) for u , we obtain the Galerkin model

$$\dot{a}_i = d_i + A_{ij}a_j + B_{ijk}a_ja_k, \quad i = 1, \dots, n, \quad (10)$$

with

$$\begin{aligned} d_i &= \langle d + A\bar{u} + B(\bar{u}, \bar{u}), \varphi_i \rangle \\ A_{ij} &= \langle A\varphi_j + 2B(\bar{u}, \varphi_j), \varphi_i \rangle \\ B_{ijk} &= \langle B(\varphi_j, \varphi_k), \varphi_i \rangle, \end{aligned} \quad (11)$$

where in (10) we use the convention that repeated indices are summed. Observe that, because of the symmetry of B , it follows that $B_{ijk} = B_{ikj}$. Also note that, in order to calculate the coefficients d_i , A_{ij} , and B_{ijk} , one needs to be able to evaluate not just f in (8), but also its separate constant, linear, and bilinear components, and thus this method is considered “intrusive.”

2.2.2 Operator Inference models

The formulation of Galerkin models described in the previous section requires explicit access to the operators of the full-order dynamics (8), in order to calculate the coefficients in (11). However, in many practical scenarios, the full model may be given as a “black box” providing only the function f (not its individual components d , A , and B), or simply a timestepper that advances $u(t)$ to $u(t + \Delta t)$.

To build reduced-order models without requiring access to the full-order operators, the operator inference method [20] offers a natural and flexible approach. The initial steps are similar to those of the Galerkin method, as we determine a reduced basis φ_i from snapshots and project the full-state trajectories onto this basis to obtain reduced variables $a_i(t_m) = \langle u(t_m) - \bar{u}, \varphi_i \rangle$. We again assume the dynamics are quadratic, as in (8), but without explicit access to these operators, we simply postulate the quadratic form of the reduced-order model as in (10), and determine the coefficients d_i , A_{ij} , and B_{ijk} by fitting to the available data.

In order to determine these coefficients, we will also require the time derivatives of the snapshots, $\partial_t u(t_m)$. If we have access to the function f , these may be computed by simply evaluating $f(u(t_m))$. If not, and if the snapshots are spaced closely enough in time, we may approximate the time derivatives using finite differences:

$$f(u(t_m)) \approx \frac{u(t_{m+1}) - u(t_m)}{t_{m+1} - t_m}.$$

From our dataset $\{u(t_m)\}$, we then define

$$a_i(t_m) = \langle u(t_m) - \bar{u}, \varphi_i \rangle, \quad f_i(t_m) = \langle f(u(t_m)), \varphi_i \rangle, \quad (12)$$

and the model parameters $\mathcal{O} = (d_i, A_{ij}, B_{ijk})$ are determined from the minimization problem

$$\min_{\mathcal{O}} \sum_{m=1}^{N_t} \sum_{i=1}^n \left[d_i + A_{ij} a_j(t_m) + B_{ijk} a_j(t_m) a_k(t_m) - f_i(t_m) \right]^2 + R(\mathcal{O}), \quad (13)$$

where $R(\mathcal{O})$ denotes a regularization function that penalizes large values of the coefficients. Observe that the parameters in \mathcal{O} appear linearly inside the square brackets, so if the regularization function is also quadratic in the parameters, then this is a least-squares problem, which is convex and has a unique minimum [20].

Finally, we note that because of the aforementioned symmetry property of the coefficients in (11), namely $B_{ijk} = B_{ikj}$, the number of optimization parameters for B_{ijk} is not n^3 , but rather $n^2(n + 1)/2$.

2.3 Symmetry reduction and the Galerkin method

The performance of reduced-order models, whether formulated via Galerkin projection or regression, depends heavily on the choice of basis functions φ_i . For shift-equivariant

systems, one can show that in order for the reduced-order model to retain this invariance property, the basis functions must be Fourier modes [7]. In order to represent localized features, typically a large number of Fourier modes is required, so reduced-order models with a small number of Fourier modes usually offer limited insight into the underlying coherent structures.

To address this limitation, a natural approach is to first remove the spatial translation from the evolution of solutions and then compute POD modes from the resulting spatially aligned solution profiles [10]. This strategy allows for a compact representation with fewer modes, from which reduced-order models can be derived to capture the essential dynamics of the spatial profiles. Once an approximation to the profile is obtained, the full solution can be reconstructed by reintroducing the spatial shift determined from the model. This methodology is the essence of the symmetry reduction technique [10, 11], also known as the method of slices [3, 12, 13]. The main contribution of this paper is to incorporate symmetry reduction into the operator inference method, and this will be described in Section 3. Before addressing this, we first give an overview of symmetry reduction with the Galerkin method.

2.3.1 Reducing the shift-equivariance symmetry

Symmetry-reduced models are based on representing a solution $u(t)$ as a shifted version of a function $\hat{u}(t)$, and this amounts to writing the equations of motion in a moving reference frame in which the translation has been removed. In terms of the shift operator S_c defined in Section 2.1, we write

$$u(t) = S_{c(t)}\hat{u}(t). \quad (14)$$

Assume for the moment that we have determined an appropriate shift amount $c(t)$ (we will discuss the choice of $c(t)$ in detail below). Then the dynamics of $\hat{u}(t)$ must satisfy

$$\begin{aligned} \partial_t \hat{u}(x, t) &= \frac{\partial}{\partial t} [u(x + c(t), t)] \\ &= \partial_t u(x + c(t), t) + \dot{c}(t) \partial_x u(x + c(t), t). \end{aligned}$$

Using the dynamics $\partial_t u = f(u)$ and writing this in terms of the shift operator, we obtain

$$\begin{aligned} \partial_t \hat{u}(t) &= S_{-c(t)} f(u(t)) + \dot{c}(t) S_{-c(t)} \partial_x u(t) \\ &= f(S_{-c(t)} u(t)) + \dot{c}(t) \partial_x S_{-c(t)} u(t), \end{aligned}$$

where we have used shift equivariance of f . Thanks to (14), this then becomes

$$\partial_t \hat{u} = f(\hat{u}) + \dot{c} \partial_x \hat{u}. \quad (15)$$

These are the dynamics in the moving reference frame; observe that the equations (15) depend only on \dot{c} , not on c itself.

We now return to the question of how to determine the shift amount $c(t)$. At each time t , we will choose the shift amount $c(t)$ so that the shifted solution $\hat{u}(t)$ is optimally “aligned” with a pre-chosen “template function” $u_0 \in \mathcal{U}$. That is, we will choose

$$c(t) = \arg \min_c \|S_{-c}u(t) - u_0\|^2, \quad (16)$$

where the norm on \mathcal{U} is the standard one induced by the inner product (6). This is equivalent to

$$\begin{aligned} c(t) &= \arg \max_c \langle S_{-c}u(t), u_0 \rangle \\ &= \arg \max_c \langle u(t), S_c u_0 \rangle. \end{aligned}$$

A necessary condition for a local maximum is therefore

$$\frac{d}{dc} \langle u(t), S_c u_0 \rangle = 0.$$

A quick calculation reveals that, for any $v \in \mathcal{U}$,

$$\frac{d}{dc} S_c[v](x) = \frac{d}{dc} v(x - c) = -\partial_x v(x - c) = -S_c[\partial_x v](x),$$

and thus the condition for a local maximum becomes

$$\begin{aligned} \langle u(t), -S_{c(t)} \partial_x u_0 \rangle &= 0 \\ \iff \langle S_{-c(t)} u(t), \partial_x u_0 \rangle &= 0 \\ \iff \langle \hat{u}(t), \partial_x u_0 \rangle &= 0. \end{aligned}$$

As explained in [11], this condition has an intuitive geometric interpretation: the shifted solution \hat{u} must lie in a subspace of \mathcal{U} orthogonal to the function $\partial_x u_0$ (this subspace is called a *slice*, hence the *method of slices* mentioned earlier).

Since this relation must hold for $\hat{u}(t)$ at every time t , we may differentiate with respect to t to obtain

$$\frac{d}{dt} \langle \hat{u}(t), \partial_x u_0 \rangle = 0,$$

and substituting the dynamics (15), we have

$$\langle f(\hat{u}) + \dot{c} \partial_x \hat{u}, \partial_x u_0 \rangle = 0.$$

Thus, solving for \dot{c} , we obtain

$$\dot{c} = -\frac{\langle f(\hat{u}), \partial_x u_0 \rangle}{\langle \partial_x \hat{u}, \partial_x u_0 \rangle}. \quad (17)$$

This expression then determines \dot{c} in the dynamics (15). Furthermore, once a solution $\hat{u}(t)$ to (15) is obtained, the shift amount $c(t)$ can be determined by integrating (17) in time, and used to reconstruct the solution $u(t)$ in the original reference frame. We therefore call (17) a “reconstruction equation,” after [11].

2.3.2 Symmetry-reduced Galerkin for quadratic dynamics

We now combine the symmetry-reduction approach, just explained, with the Galerkin method from Section 2.2.1. We consider again quadratic dynamics

$$\partial_t u(t) = f(u(t)) = d + Au(t) + B(u(t), u(t)) \quad (18)$$

and write $u(t) = S_{c(t)}\hat{u}(t)$, with

$$\hat{u}(t) = \bar{u} + \sum_{i=1}^n a_i(t)\varphi_i, \quad (19)$$

where $\bar{u} \in \mathcal{U}$ is again the mean, and $\varphi_i \in \mathcal{U}$ are again orthonormal basis functions. The time evolution of $\hat{u}(t)$ is then determined by (15), and Galerkin projection gives

$$\langle \partial_t \hat{u}(t), \varphi_i \rangle = \langle f(\hat{u}(t)) + \dot{c} \partial_x \hat{u}, \varphi_i \rangle, \quad (20)$$

where \dot{c} is given by (17). Inserting our expansion (19), and using orthogonality of φ_i , we obtain

$$\dot{a}_i(t) = d_i + A_{ij}a_j(t) + B_{ijk}a_j(t)a_k(t) + \dot{c}(b_i + C_{ij}a_j(t)), \quad (21)$$

for $i = 1, \dots, n$, where we again employ the summation convention, and coefficients are given by (11), together with

$$\begin{aligned} b_i &= \langle \partial_x \bar{u}, \varphi_i \rangle \\ C_{ij} &= \langle \partial_x \varphi_j, \varphi_i \rangle, \end{aligned} \quad (22)$$

and \dot{c} has the form

$$\dot{c} = -\frac{e + p_j a_j(t) + Q_{jk} a_j(t) a_k(t)}{w + s_j a_j(t)}, \quad (23)$$

with

$$\begin{aligned} e &= \langle d + A\bar{u} + B(\bar{u}, \bar{u}), \partial_x u_0 \rangle \\ p_j &= \langle A\varphi_j + 2B(\bar{u}, \varphi_j), \partial_x u_0 \rangle \\ Q_{jk} &= \langle B(\varphi_j, \varphi_k), \partial_x u_0 \rangle \\ w &= \langle \partial_x \bar{u}, \partial_x u_0 \rangle \\ s_j &= \langle \partial_x \varphi_j, \partial_x u_0 \rangle \end{aligned} \quad (24)$$

Observe that there is a symmetry in the coefficients $Q_{jk} = Q_{kj}$, because of the symmetry of B . Like the Galerkin method discussed in Section 2.2.1, this method is intrusive,

as one needs access to d , A , and B from the full dynamics (18) in order to compute the coefficients. Our objective in the next section is to obtain a non-intrusive method.

3 Symmetry-reduced operator inference

We now describe the main contribution of this paper, a method combining symmetry reduction with operator inference. We first describe a baseline approach with a naive non-intrusive approximation of the shifting speed $\dot{c}(t)$, and show its limitations. We then describe our proposed method, which incorporates additional operators into the reduced-order model. Finally, we describe a snapshot preprocessing strategy based on the re-projection technique [28], which enables our non-intrusive method to converge to its intrusive counterpart, the symmetry-reduced Galerkin model.

3.1 Basic formulation and its drawbacks

In standard operator inference described in Section 2.2.2, one learns coefficients d_i , A_{ij} , and B_{ijk} , from which we can assemble

$$f_i(a) = d_i + A_{ij}a_j + B_{ijk}a_ja_k, \quad (25)$$

and the coefficients $a_i(t)$ of the reduced-order model evolve according to $\dot{a}_i = f_i(a)$. In order to combine this with the symmetry-reduction ideas described in Section 2.3, perhaps the simplest idea is the following: given the reduced variables $a = (a_1, \dots, a_n)$, reconstruct the approximations of \hat{u} and $f(\hat{u})$ in the full space, and use these to determine the shift amount \dot{c} , from (17).

To make this precise, we define

$$\tilde{f}(a) = \sum_{i=1}^n f_i(a)\varphi_i, \quad \tilde{u}(a) = \bar{u} + \sum_{i=1}^n a_i\varphi_i, \quad (26)$$

and let \dot{c} be given by

$$\dot{c} = -\frac{\langle \tilde{f}(a), \partial_x u_0 \rangle}{\langle \partial_x \tilde{u}(a), \partial_x u_0 \rangle}. \quad (27)$$

The numerator of \dot{c} is quadratic in the variables a_i , and depends on the coefficients d_i , A_{ij} , and B_{ijk} , which are learned in the operator inference procedure, while the denominator is linear in the variables a_i , and has known coefficients, given by (24).

Once \dot{c} is known, the reduced-order model (21) can be used to determine the dynamics of the reduced state $a(t)$.

This procedure has a subtle but serious flaw: the functions $f(\hat{u})$ often do not lie in the subspace that \hat{u} lies in, and this can result in drastically incorrect approximations of the shift speed \dot{c} .

As an illustrative example, consider the advection-diffusion equation

$$\partial_t u + a \partial_x u = \partial_x^2 u, \quad (28)$$

in a periodic (or infinite) domain. The shift speed determined by equation (17) is

$$\dot{c} = -\frac{\langle -a \partial_x \hat{u} + \partial_x^2 \hat{u}, \partial_x u_0 \rangle}{\langle \partial_x \hat{u}, \partial_x u_0 \rangle} = a + \frac{\langle \partial_x^2 \hat{u}, \partial_x u_0 \rangle}{\langle \partial_x \hat{u}, \partial_x u_0 \rangle}.$$

Now, suppose the initial condition is an even function $u(x, 0) = g(x)$, where $g(-x) = g(x)$, and suppose the template function u_0 is also even. Then $\partial_x u_0$ is odd and $\partial_x^2 \hat{u}$ is even, so the numerator in the last term above is zero, and the shift speed is simply $\dot{c} = a$. Furthermore, the dynamics of \hat{u} as given by (15) are

$$\partial_t \hat{u} = \partial_x^2 \hat{u}, \tag{29}$$

a simple diffusion equation. The shifting procedure has removed the advection part of the equation, as desired.

Now, since the initial condition is an even function, the solution $\hat{u}(t)$ of (29) will remain even for all time (as $\partial_x^2 \hat{u}$ is even), so our basis functions φ_i (for instance, determined by POD) will also be even functions. Thus, if we determine $\tilde{f}(a)$ according to (26), then $\tilde{f}(a)$ will be even as well. But then in our approximation of \dot{c} in (27), the numerator consists of the inner product between an even function (\tilde{f}) and an odd function ($\partial_x u_0$). Since even and odd functions are orthogonal, the shift speed predicted by our model will always be zero!

One solution could be to consider a larger subspace, which captures $f(\hat{u})$ as well as \hat{u} : for instance, if one uses POD to determine the basis functions φ_i , one could include snapshots of $f(u(t_m))$ in addition to snapshots of $u(t_m)$. However, this would result in a larger-dimensional subspace, and a less “efficient” reduced-order model. Below we take a different approach.

3.2 An improved version of Symmetry-Reduced Operator Inference

As we have seen, approximating the shift speed \dot{c} according to (27) has serious drawbacks. To address these, we propose learning a model for \dot{c} at the same time that we learn the model for f_i in (25). In particular, since we know the true \dot{c} has the form (23), we consider a model of the form

$$\dot{c}(a) = -\frac{e + p_j a_j + Q_{jk} a_j a_k}{w + s_j a_j}, \tag{30}$$

in which the coefficients w and s_j are known, and can be computed from (24), while the coefficients e , p_j , Q_{jk} need to be learned from the data. Because of the symmetry $Q_{jk} = Q_{kj}$, the number of additional parameters to learn is $1 + n + n(n + 1)/2$.

For a given dataset $\{u(t_m)\}$, we begin by aligning the data to a template function $u_0 \in \mathcal{U}$, to obtain shifted snapshots $\hat{u}(t_m)$ and shifting speeds $\dot{c}(t_m) = \dot{c}(\hat{u}(t_m))$ for our dataset. As with standard operator inference (12), we project the (shifted) snapshots

and their time derivatives, to define

$$a_i(t_m) = \langle \hat{u}(t_m) - \bar{u}, \varphi_i \rangle, \quad f_i(t_m) = \langle f(\hat{u}(t_m)), \varphi_i \rangle, \quad (31)$$

noting that

$$f(\hat{u}(t_m)) = f(S_{-c(t_m)}u(t_m)) = S_{-c(t_m)}f(u(t_m)), \quad (32)$$

because of the shift-equivariance of f . Let

$$r_i(t_m) = \langle \partial_x \hat{u}(t_m), \varphi_i \rangle \quad (33)$$

and then the parameters $\mathcal{O} = (d_i, A_{ij}, B_{ijk}, e, p_j, Q_{jk})$ are determined by solving the minimization problem

$$\begin{aligned} \min_{\mathcal{O}} \sum_{m=1}^{N_t} \sum_{i=1}^n \left\{ \left[d_i + A_{ij}a_j(t_m) + B_{ijk}a_j(t_m)a_k(t_m) - f_i(t_m) \right]^2 \right. \\ \left. + \lambda \left[- \frac{e + p_j a_j(t_m) + Q_{jk} a_j(t_m) a_k(t_m)}{w + s_j a_j(t_m)} (b_i + C_{ij} a_j(t_m)) - \dot{c}(t_m) r_i(t_m) \right]^2 \right\} + R(\mathcal{O}), \end{aligned} \quad (34)$$

where the parameters $b_i, C_{ij}, w,$ and s_j are given explicitly by (22) and (24), and $\lambda > 0$ is a hyperparameter used to balance the relative weight of the two error terms.

It is straightforward to show that the optimization problem (34) is convex, under the same conditions that the original operator inference problem (13) is convex, and thus has a global minimum. While the approach here does involve more optimization parameters than the original operator inference problem, the number of additional parameters $(1 + n + n(n + 1)/2)$ is small compared with the number of the parameters in the original operator inference problems (which is more than $n^2(n + 1)/2$).

The final reduced-order model is then given by

$$\dot{a}_i(t) = d_i + A_{ij}a_j(t) + B_{ijk}a_j(t)a_k(t) + \dot{c}(a)(b_i + C_{ij}a_j(t)), \quad (35)$$

with $\dot{c}(a)$ given by (30). Algorithm 1 summarizes all of the steps involved in our symmetry-reduced operator inference procedure, which we call SR-OpInf.

3.3 Re-projection and convergence of SR-OpInf to SR-Galerkin

Since intrusive symmetry-reduced Galerkin ROMs are known to capture the essential dynamics of traveling solutions effectively, it is natural to ask whether a symmetry-reduced ROM learned via operator inference converges to the SR-Galerkin ROM with projection-based reduced operators as more data are provided. The answer, as explained in [28], is in general no. However, this reference also proposes a modification to the training dataset for the operator inference method, known as *re-projection*. When this technique is applied, the learned model converges to the (intrusive) Galerkin model. Here, we show how to apply the re-projection technique to our symmetry-reduced OpInf procedure.

Algorithm 1 The learning algorithm of Symmetry-Reduced Operator Inference

Require: Snapshots of the solution $u(t_m) \in \mathcal{U}$ and the velocities $f(u(t_m)) \in \mathcal{U}$, $m = 1, \dots, N_t$. The template function $u_0 \in \mathcal{U}$ for template fitting. The dimension of the desired reduced-order model $n \leq N$.

Ensure: The Symmetry-Reduced Operator Inference model (35), (30) describing the time evolution of the reduced state $a(t) = (a_1(t), \dots, a_n(t))$.

- 1: **for** $m = 1, \dots, N_t$ **do**
 - 2: Perform template fitting to obtain the shifted snapshots $\hat{u}(t_m)$ and the corresponding velocities $f(\hat{u}(t_m))$ according to (14), (16), and (32).
 - 3: Determine the shifting speed $\dot{c}(t_m) = \dot{c}(\hat{u}(t_m))$ from (17).
 - 4: **end for**
 - 5: Calculate the mean of the shifted snapshots $\hat{u}(t_m)$, from (5).
 - 6: Perform POD on the set of centered snapshots $\{\hat{u}(t_m) - \bar{u}\}$, to obtain orthonormal basis functions $\varphi_i \in \mathcal{U}$, $i = 1, \dots, n$.
 - 7: **for** $m = 1, \dots, N_t$ **do**
 - 8: Determine $a_i(t_m)$ and $f_i(t_m)$ from (31), and $r_i(t_m)$ from (33).
 - 9: **end for**
 - 10: Determine the coefficients w , s_j from (24), and b_i , C_{ij} from (22).
 - 11: Learn the coefficients d_i , A_{ij} , B_{ijk} , e , p_j , and Q_{jk} by solving the optimization problem (34) (noting the symmetry, $B_{ijk} = B_{ikj}$ and $Q_{jk} = Q_{kj}$).
 - 12: The reduced-order model is given by (35) with \dot{c} given by (30).
-

In order to apply re-projections, given shifted snapshots $\hat{u}(t_m)$ and a set of basis functions φ_i , we first form the (affine) projection

$$P\hat{u}(t) = \bar{u} + \sum_i \langle \hat{u}(t) - \bar{u}, \varphi_i \rangle \varphi_i, \quad (36)$$

where \bar{u} is the mean of shifted snapshots.

Next, we apply the re-projection technique starting from a (new) initial condition $u(0)$ suitable for constructing the re-projected dataset. The procedure proceeds iteratively with each step indexed by $p = 0, 1, \dots, N_T - 1$ corresponding to the time $t = p\Delta t$, where Δt is the timestep of the FOM timestepper $F_{\Delta t} : u(t) \mapsto u(t + \Delta t)$. At the p_{th} step, we begin with shifting the current FOM solution $u(t)$ to align with the template function u_0 :

$$\hat{u}(t) = S_{-c_{\text{RP}}(t)} u(t), \quad (37)$$

with the shifting amount determined using (16). Next, we perform the affine projection of the shifted state onto the reduced subspace, from which we obtain the shifted re-projected snapshot:

$$\hat{u}_{\text{RP}}(t) = P\hat{u}(t). \quad (38)$$

This re-projected state $\hat{u}_{\text{RP}}(t)$ is used to advance the FOM timestepper such that:

$$u(t + \Delta t) = F_{\Delta t}(\hat{u}_{\text{RP}}(t)). \quad (39)$$

If the velocity f is available from the FOM, we evaluate it directly at the shifted re-projected state as $f(\hat{u}_{\text{RP}}(t))$. Otherwise, we approximate the velocity via finite

differencing:

$$f(\hat{u}_{\text{RP}}(t)) \approx \frac{F_{\Delta t}(\hat{u}_{\text{RP}}(t)) - \hat{u}_{\text{RP}}(t)}{\Delta t}. \quad (40)$$

Finally, we define the re-projected shifting speed as

$$\dot{c}_{\text{RP}}(t) = \dot{c}(\hat{u}_{\text{RP}}(t)) = -\frac{\langle f(\hat{u}_{\text{RP}}(t)), \partial_x u_0 \rangle}{\langle \partial_x \hat{u}_{\text{RP}}(t), \partial_x u_0 \rangle}. \quad (41)$$

After completing all N_T steps, we arbitrarily select N_t indices $\{p_1, p_2, \dots, p_{N_t}\} \subseteq \{0, 1, \dots, N_T - 1\}$ with associated sampling times given by $t_m = p_m \Delta t$ for $m = 1, 2, \dots, N_t$. For each t_m , we sample a tuple consisting of the shifted solution $\hat{u}_{\text{RP}}(t_m)$ from (38), the corresponding velocity $f(\hat{u}_{\text{RP}}(t_m))$ either from the FOM output or via finite differencing (40), and the shifting speed $\dot{c}_{\text{RP}}(t_m)$ from (41). These data $\{\hat{u}_{\text{RP}}(t_m), f(\hat{u}_{\text{RP}}(t_m)), \dot{c}_{\text{RP}}(t_m)\}_{m=1}^{N_t}$ can then be directly used to compute the quantities $a_i(t_m)$, $f_i(t_m)$ and $r_i(t_m)$ in the loss function (34) following the definitions in (31) and (33). This bypasses the need for repeated template fitting or re-computing a new set of POD modes from the re-projected snapshots. As shown in [28], OpInf ROMs trained on re-projected data converge to the intrusive Galerkin ROMs under suitable conditions. The same conclusion holds in the symmetry-reduced setting: if we calculate $a_i(t_m)$, $f_i(t_m)$ and $r_i(t_m)$ from the re-projected dataset using (31) and (33) while substituting the shifting speed $\dot{c}(t_m)$ in (34) with the re-projected value $\dot{c}_{\text{RP}}(t_m)$, then the loss function attains zero. Consequently, the inferred operators \mathcal{O} exactly match those obtained from symmetry-reduced Galerkin projection. We summarize the learning algorithm incorporated with the re-projection technique in Algorithm 2.

Remark 1 The convergence of the SR-OpInf ROM to the SR-Galerkin ROM is guaranteed when the re-projected velocity $f(\hat{u}_{\text{RP}}(t))$ is directly accessible from the FOM or can be accurately computed via finite differencing. If its actual value is not available, then exact convergence is not guaranteed. Nevertheless, as the FOM timestep $\Delta t \rightarrow 0$, the finite difference approximation of f becomes increasingly accurate, and the discrepancy between the learned model and the Galerkin model decreases [20].

4 Results

In this work, we apply the proposed SR-OpInf ROM to perform model reduction on a representative shift-equivariant PDE system: the Kuramoto–Sivashinsky equation (KSE), given by

$$\partial_t u = f(u) = -u \partial_x u - \partial_x^2 u - \nu \partial_x^4 u, \quad (42)$$

on the domain $x \in [0, 2\pi]$ with periodic boundary conditions. The function f is thus of the form (8) with

$$d = 0, \quad Au = -\partial_x^2 u - \nu \partial_x^4 u, \quad B(u, v) = -\frac{1}{2}(u \partial_x v + v \partial_x u).$$

Algorithm 2 The learning algorithm of SR-OpInf ROM with re-projection technique

Require: Non-reprojected snapshots of the solution $u(t_m) \in \mathcal{U}$. The dimension of the ROM n . The template function $u_0 \in \mathcal{U}$ for template fitting. An initial condition $u(0) \in \mathcal{U}$ suitable for constructing the re-projected training dataset. A large enough number of total timesteps N_T for FOM simulation during the re-projection.

Ensure: The Symmetry-Reduced Operator Inference model (35), (30) trained on the re-projected dataset $\{\hat{u}_{\text{RP}}(t_m), f(\hat{u}_{\text{RP}}(t_m)), \dot{c}_{\text{RP}}(t_m)\}_{m=1}^{N_t}$.

- 1: **for** $m = 1, \dots, N_t$ **do**
 - 2: Perform template fitting to obtain the shifted non-reprojected snapshots $\hat{u}(t_m)$ from $u(t_m)$ according to (14) and (16).
 - 3: **end for**
 - 4: Calculate the mean \bar{u} of the shifted non-reprojected snapshots $\hat{u}(t_m)$ from (5).
 - 5: Perform POD on the set of centered snapshots $\{\hat{u}(t_m) - \bar{u}\}_{m=1}^{N_t}$, to obtain orthonormal basis functions $\varphi_i \in \mathcal{U}$, $i = 1, \dots, n$.
 - 6: Determine the coefficients w , s_j , b_i and C_{ij} in the SR-OpInf ROM from (24) and (22).
 - 7: Apply the re-projection technique to construct the re-projected dataset:
 - 8: Pick a (new) initial condition $u(0)$ for constructing the re-projected dataset.
 - 9: **for** $p = 0, \dots, N_T - 1$ **do**
 - 10: Denote $t = p\Delta t$.
 - 11: Shift the current FOM solution $u(t)$ to align it with the template via (16), resulting in the shifted profile $\hat{u}(t)$.
 - 12: Project $\hat{u}(t)$ onto the affine reduced subspace following (36) to obtain the shifted re-projected solution $\hat{u}_{\text{RP}}(t)$.
 - 13: Call the FOM timestepper to obtain the FOM state at the next timestep $u(t + \Delta t)$ following (39).
 - 14: Calculate the corresponding velocity $f(\hat{u}_{\text{RP}}(t))$ from the output of FOM or finite-differencing approximation (40).
 - 15: Compute the re-projected shifting speed $\dot{c}_{\text{RP}}(t)$ via (41).
 - 16: **end for**
 - 17: Select N_t indices $\{p_1, p_2, \dots, p_{N_t}\} \subseteq \{0, 1, \dots, N_T - 1\}$ with associated sampling times $t_m = p_m\Delta t$ for $m = 1, 2, \dots, N_t$. For each t_m , collect $\hat{u}_{\text{RP}}(t_m)$, $f(\hat{u}_{\text{RP}}(t_m))$, and $\dot{c}_{\text{RP}}(t_m)$ to form the re-projected training dataset.
 - 18: **for** $m = 1, \dots, N_t$ **do**
 - 19: Determine $a_i(t_m)$, $f_i(t_m)$, and $r_i(t_m)$ from the re-projected dataset using (31) and (33).
 - 20: **end for**
 - 21: Learn the coefficients d_i , A_{ij} , B_{ijk} , e , p_j , and Q_{jk} by solving the optimization problem (34) (noting the symmetry, $B_{ijk} = B_{ikj}$ and $Q_{jk} = Q_{kj}$).
 - 22: The reduced-order model is given by (35) with \dot{c} given by (30).
-

The linear part of the KSE consists of a destabilizing second-order term $-\partial_x^2 u$ and a stabilizing fourth-order hyper-diffusion term $-\nu \partial_x^4 u$. This combination implies that low-wavenumber modes are linearly unstable, while high-wavenumber modes are linearly damped. As a result, the KSE exhibits dynamics qualitatively similar to the energy cascade in three-dimensional turbulence governed by the Navier–Stokes equations, and is often referred to as a model for “one-dimensional turbulence” [29]. Another key reason for the widespread use of the KSE in reduced-order modeling lies in its rich solution dynamics, especially in the parameter regime $\nu \in (4/89, 2/43)$ where the system exhibits a variety of solutions with low-order dynamics [30]. In this work, we focus on the globally shifting, beating-wave periodic solutions as a particular class of such solutions and collect their snapshots as the training data for our ROMs. These solutions make the KSE an ideal testbed for evaluating ROMs designed to handle high-dimensional shift-equivariant systems with spatial drifting solutions.

In this section, we begin by computing a high-fidelity numerical solution of (42) for a specific value of ν to generate the training dataset; see Section 4.1 for full details. We then construct multiple ROMs and evaluate their performance in reconstructing the data using several quantitative metrics. Finally, we assess the SR-OpInf ROM on a testing dataset to validate its ability to preserve the shift-equivariance property of the original full-order model.

4.1 Numerical details

To collect the training dataset featuring snapshots of shifting beating-wave solution, we first simulate (42) at $\nu = 4/87$ using a spectral Galerkin method with 20 complex Fourier modes. We use a semi-implicit timestepper [31, 32] for time integration with a Crank-Nicholson scheme for the linear terms and a third-order explicit Runge-Kutta scheme for the nonlinear term. The initial condition chosen to induce a globally shifting solution is given by [10, 11]

$$u(0) = -\sin(x) + 2\cos(2x) + 3\cos(3x) - 4\sin(4x). \quad (43)$$

Through the convergence study, we determine that a timestep $\Delta t_{\text{FOM}} = 10^{-3}$ is sufficient to compute the solution.

Next, we formulate the non-reprojected dataset $\{u(t_m), f(u(t_m)), \dot{c}(t_m)\}_{m=1}^{N_t}$ collecting temporally equispaced snapshots from $t_1 = 120$ to $t_{N_t} = 130$ after the transient, with a sample interval $\Delta t_s = 0.01$ resulting in $N_t = 1001$. For simplicity, we assume that the velocity f is available from the FOM. To obtain the template fitted snapshots $\hat{u}(t_m)$ and $f(\hat{u}(t_m))$, we choose the template function $u_0(x) = \cos(x)$ as the real part of the first Fourier mode following previous studies on symmetry reduction of shift-equivariant spatially extended systems [13]. Using this, we compute the template fitted profiles $\hat{u}(t_m) = S_{-c(t_m)}u(t_m)$ and $f(\hat{u}(t_m))$, and calculate the shifting speed $\dot{c}(t_m)$ via the reconstruction equation (17). The shifting operator S_{-c} acting on $u(t)$ is implemented in the Fourier domain by multiplying each Fourier coefficient of $u(t)$ by $\exp(ik(-c))$, where k is the corresponding wavenumber and c is the shifting amount. These tuples $\{(\hat{u}(t_m), f(\hat{u}(t_m)), \dot{c}(t_m))\}_{m=1}^{N_t}$ form the training dataset from which we extract dominant POD modes as the reduced basis and learn the reduced operators.

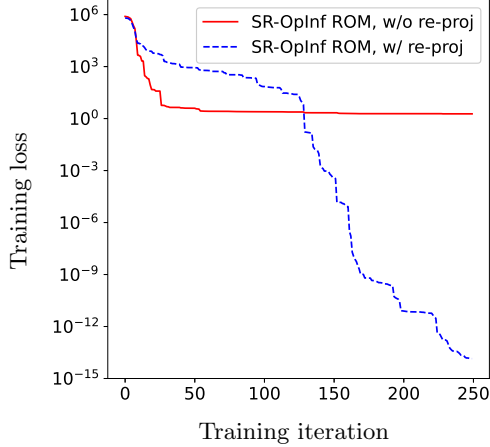


Fig. 1: Training losses of 4-mode SR-OpInf ROMs with different training datasets. The red solid line (—) displays the training loss (34) with non-reprojected dataset $\{(\hat{u}(t_m), f(\hat{u}(t_m)), \dot{c}(t_m))\}_{m=1}^{N_t}$, with the loss plateauing at ≈ 1.648 after 100 iteration steps. The blue dashed line (---) shows the training loss with the re-projected dataset $\{(\hat{u}_{RP}(t_m), f(\hat{u}_{RP}(t_m)), \dot{c}_{RP}(t_m))\}_{m=1}^{N_t}$, which converges to a level of 10^{-15} after 250 steps.

We consider three ROMs in this study, all constructed using the same reduced basis consisting of $n = 4$ POD modes: the SR-OpInf ROM trained on non-reprojected dataset $\{(\hat{u}(t_m), f(\hat{u}(t_m)), \dot{c}(t_m))\}_{m=1}^{N_t}$ following Algorithm 1, the SR-OpInf ROM trained on reprojected dataset $\{(\hat{u}_{RP}(t_m), f(\hat{u}_{RP}(t_m)), \dot{c}_{RP}(t_m))\}_{m=1}^{N_t}$ following Algorithm 2, and the intrusive SR-Galerkin ROM obtained via Galerkin projection onto the reduced basis. We construct the re-projected dataset following Algorithm 2, using the first non-reprojected snapshot as the new initial condition $u(0) = u(t_1)$ and evolving over the same time length as the original dataset. We keep the sampling interval unchanged to ensure that the number of re-projected snapshots matches that of the non-reprojected ones. To ensure exact convergence of the SR-OpInf ROM trained on the re-projected dataset to its intrusive SR-Galerkin counterpart, we omit the regularizer $\mathcal{R}(\mathcal{O})$ from the minimization problem (34), following the convention in [28]. This choice better isolates the effect of the re-projection technique in improving the training dataset, thereby enhancing the stability and robustness of the learned SR-OpInf ROM and promoting its alignment with the SR-Galerkin ROM, which is already known for its strong performance. We do not include the standard Galerkin ROM, as it has previously been shown to perform poorly in this setting—for example, an 8-mode Galerkin ROM is significantly outperformed by a 3-mode SR-Galerkin ROM [10, 11]. Likewise, the standard OpInf ROM is excluded since it cannot be expected to significantly outperform the Galerkin ROM [28].

We solve the SR-OpInf optimization problem (34) using the conjugate gradient algorithm, which provides efficient and robust updates for large-scale least-squares

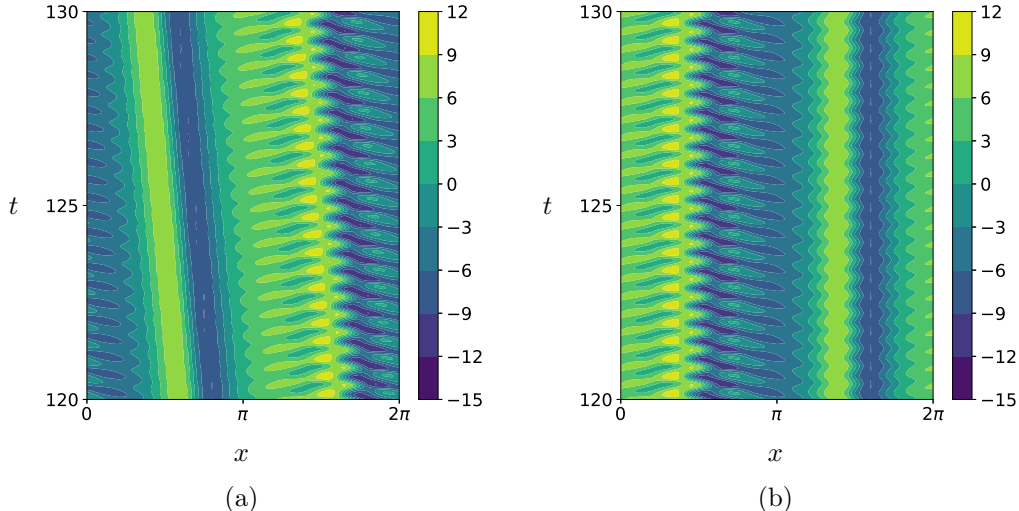


Fig. 2: The full-order solution $u(t)$ to (42) at $\nu = 4/87$ exhibiting upstream traveling beating patterns. Panel (a) displays $u(t)$ in the original frame and panel (b) shows the shifted version $\hat{u}(t)$ after the template fitting process with the template $u_0(x) = \cos(x)$. The contour plots are generated by sampling $u(t)$ on a grid of $[0, 2\pi]$ with $N = 40$ equispaced points.

problems. This approach avoids explicitly forming and inverting large, potentially ill-conditioned data matrices that would otherwise be required for directly computing the minimizer (as discussed in [20, 28]). Given the global convergence properties of the problem, we initialize all entries in $\mathcal{O} = (d_i, A_{ij}, B_{ijk}, e, p_i, Q_{ij})$ to 0 and set the hyperparameter $\lambda = 1$. As shown in Fig. 1, the SR-OpInf ROM consisting of $n = 4$ POD modes trained on reprojected data achieves a training loss on the order of 10^{-15} after 250 steps, which is effectively 0. In contrast, training with the non-reprojected snapshots results in a $O(10^0)$ level of loss. This discrepancy arises from the intrinsic non-Markovian structure of the full-order dynamics projected onto a low-dimensional subspace, which cannot be accurately captured by projection-based ROMs without pre-processing such as re-projection [28].

Once trained, the ROM is used to reconstruct the original dataset. We integrate the reduced system following the conventions of [11] using a Runge–Kutta–Fehlberg (RKF45) method [33] with adaptive time stepping and a local error tolerance of 10^{-6} . The initial timestep is set to $\Delta t_{\text{ROM}} = 10^{-3} = \Delta t_{\text{FOM}}$, and a lower bound $\Delta t_{\text{ROM}} \geq 10^{-5}$ is imposed; if the adaptive step falls below this threshold, the ROM simulation is considered numerically unstable and is terminated.

4.2 Model predictions via SR-OpInf and other ROMs

We now evaluate the performance of the SR-OpInf ROM trained on re-projected data in reconstructing the full-order solution $u(t)$ and the shifting speed $\dot{c}(t)$. Fig. 2 displays

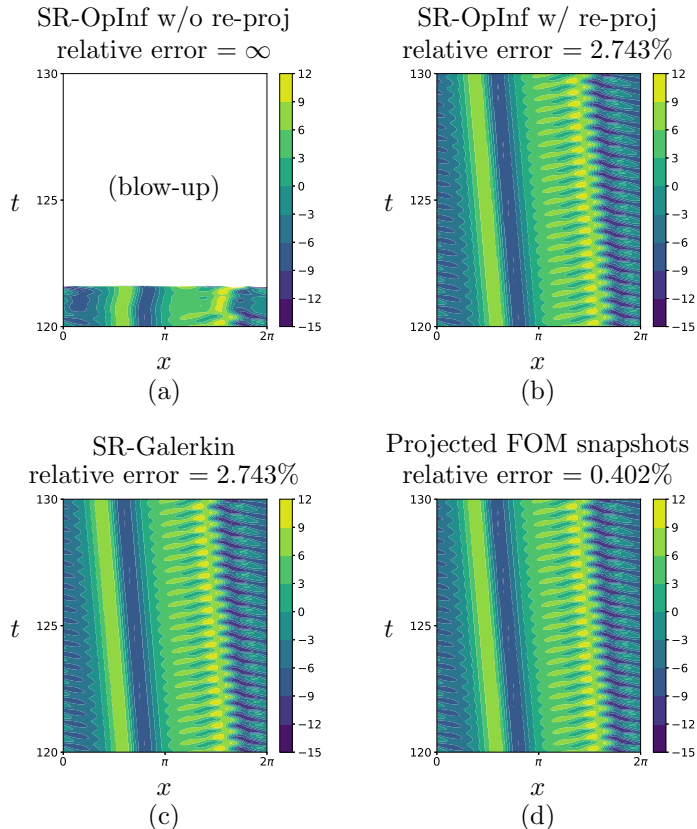


Fig. 3: Reconstructions of the training snapshots $\{u(t_m)\}_{m=1}^{N_t}$ given by (a) the SR-OpInf ROM trained from the non-reprojected dataset (b) the SR-OpInf ROM trained from the reprojected dataset (c) the SR-Galerkin ROM and (d) the affine projection (36) onto the reduced basis $S_{c(t_m)}PS_{-c(t_m)}u(t_m)$. All results are computed with the same reduced basis φ_i consisting of $n = 4$ POD modes. The relative error is as defined in (44).

the FOM snapshots $\{u(t_m)\}_{m=1}^{N_t}$ before and after applying the template fitting procedure. The original solution (Fig. 2a) exhibits upstream-traveling beating waves. After template fitting with the assigned template, the dominant trend of leftward motion is largely removed, though some residual “zig-zagging” remains in the fitted snapshots (Fig. 2b). This irregularity reflects the fact that the template fitting algorithm only minimizes the L^2 -distance to the template and does not account for time-varying changes in the wave profile, potentially introducing spurious shifts when the profile deforms. Nonetheless, the dominant drift is effectively neutralized.

We then evaluate how well each ROM reconstructs the FOM training snapshots using the first snapshot $u(t_1)$ as the initial condition. To quantify the discrepancies

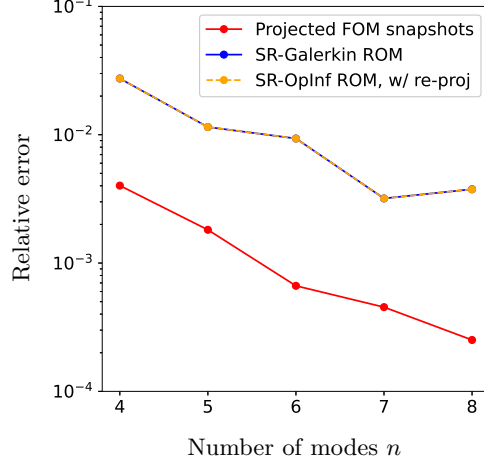


Fig. 4: Relative errors of the projected FOM snapshots (red solid line —), the predicted snapshots from the SR-Galerkin ROM (blue solid line —), and the predicted snapshots from the SR-OpInf ROM trained on the re-projected dataset (orange dashed line - - -) for various dimensions of the reduced basis $n = 4, 5, 6, 7$, and 8.

between ROM prediction $u_{\text{ROM}}(t)$ and FOM data $u(t)$, we introduce the normalized error defined as follows

$$\text{relative error} = \sqrt{\frac{\sum_{m=1}^{N_t} \|u_{\text{ROM}}(t_m) - u(t_m)\|^2}{\sum_{m=1}^{N_t} \|u(t_m)\|^2}}. \quad (44)$$

Fig. 3 shows contour plots comparing $u(t)$ obtained from all models. Without the regularizer in the loss function or the re-projection technique, the SR-OpInf ROM trained on raw data (Fig. 3a) fails to accurately reproduce the upstream drift or oscillatory patterns and diverges rapidly at $t \approx 121.8$. In contrast, the SR-OpInf ROM trained on re-projected data (Fig. 3b) remains stable throughout the trajectory and successfully captures the spatial drift and wave modulation, achieving a relative error of 2.743% despite still deactivating any regularizer in the training process. The SR-Galerkin ROM (Fig. 3c) yields a comparable performance with the same relative error 2.743%, which supports that using re-projected data leads to convergence of the SR-OpInf ROM towards its intrusive Galerkin counterpart. These results highlight both the strong performance of the SR-OpInf ROM and the ameliorating effect of the re-projection technique in improving stability and accuracy, even in the absence of explicit regularization. To further evaluate the robustness of the proposed framework, we vary the dimension of the reduced state. As shown in Fig. 4, the prediction error of the SR-OpInf ROM decreases from 2.743% with $n = 4$ POD modes to 0.319% at $n = 7$ while closely matching that of the intrusive SR-Galerkin ROM across all tested dimensions. Compared to the projection errors onto the reduced basis, the prediction errors are not significantly larger. This indicates that the SR-OpInf ROM achieves

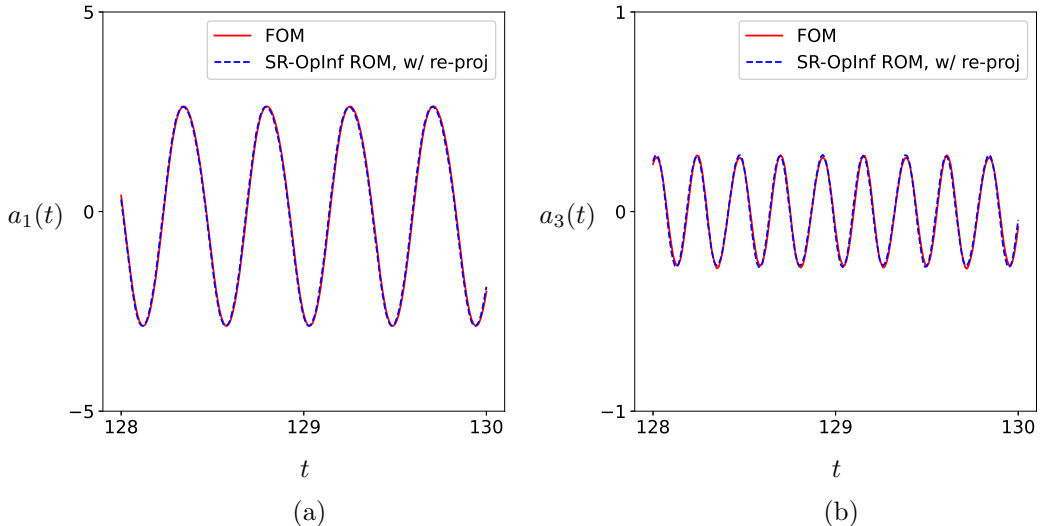


Fig. 5: Amplitudes of (a) the first POD mode $a_1(t)$ and (b) the third POD mode $a_3(t)$ during $t \in [128, 130]$. The red solid line (—) shows the FOM trajectory projected onto the reduced basis. The blue dashed line (---) shows the result from the 4-mode SR-OpInf ROM trained on the re-projected dataset.

strong and robust performance in reliably capturing the essential dynamics of the FOM. We also notice a slight increase in error beyond $n = 7$, which likely reflects the growing numerical sensitivity of the training process with respect to the size of the reduced operators [28].

Compared to the low-dimensional projection of these snapshots onto the reduced subspace (Fig. 3d) with a 0.402% projection error, the higher prediction error of SR-OpInf ROM may arise from inaccuracies in predicting the solution profiles or the shifting speeds. To isolate the source of this error, we first examine potential mismatches in the profiles by comparing the time evolution of the reduced variable $a_i(t)$, i.e., the amplitudes of POD modes, obtained from the FOM and predicted by the ROM. Fig. 5 displays the first and third components of the reduced state vector, $a_1(t)$ and $a_3(t)$, respectively, comparing the trajectories extracted from the FOM snapshots with those predicted by the SR-OpInf ROM. The second component $a_2(t)$ is omitted since its temporal evolution closely resembles that of $a_1(t)$. For clarity of visualization, we restrict the comparison to the final part of the training interval from $t = 128$ to 130 to highlight any discrepancies as time progresses. The results show that the FOM and SR-OpInf ROM produce nearly identical reduced trajectories with negligible phase misalign and amplitude error. Such level of accuracy again demonstrates that the SR-OpInf model is highly effective in reconstructing the profiles of the beating-wave pattern using only a small number of spatial modes.

Next, we examine the shifting speed $\dot{c}(t)$ and shifting amount $c(t)$ computed from the snapshots of FOM and predicted by the SR-OpInf ROM. In the FOM case, we first

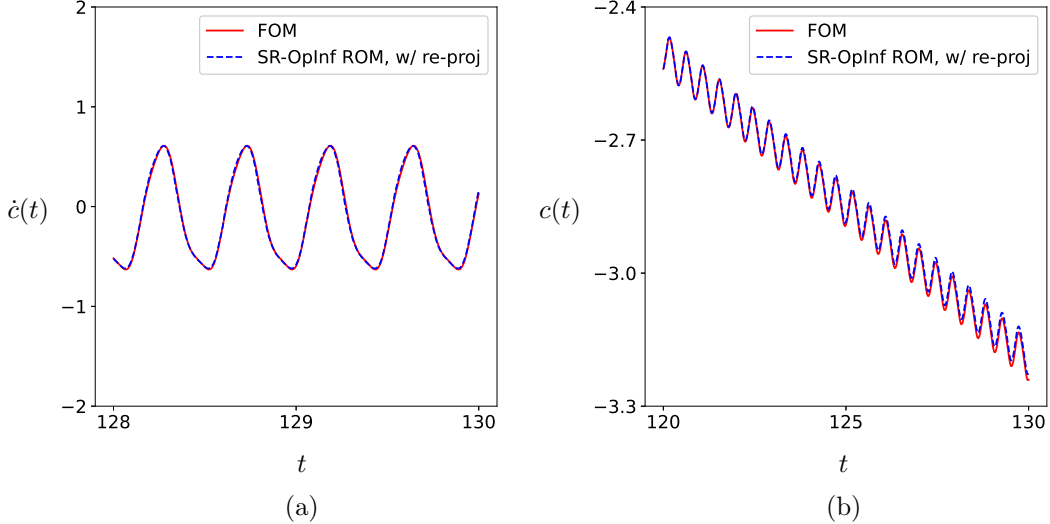


Fig. 6: Panel (a): The shifting speed $\dot{c}(t)$ of traveling solutions during $t \in [128, 130]$. Panel (b): The shifting amount $c(t)$ of traveling solutions during $t \in [120, 130]$. The red solid lines (—) represent the shifting speeds and amounts obtained from FOM snapshots using template fitting (16) and the full-order reconstruction equation (17). The blue dashed lines (---) represent the shifting speed computed from the learned reduced-order reconstruction equation (30) and the shifting amount obtained via time integration (45).

determine $c(t)$ via template fitting (16), and then compute $\dot{c}(t)$ using the full-order reconstruction equation (17). For the ROM, we first calculate $\dot{c}(t)$ via the reduced-order form of the reconstruction equation (30). We then integrate $\dot{c}(t)$ in time to get the shifting amount via a first-order timestepping scheme

$$c(t + \Delta t) = c(t) + \int_t^{t+\Delta t} \dot{c}(\tau) d\tau \approx c(t) + \dot{c}(t)\Delta t. \quad (45)$$

Fig. 6a shows the shifting speeds $\dot{c}(t)$ over the same segment $t \in [128, 130]$ of the training window. Within this time interval, all the models yield visually indistinguishable results. However, when examining the shifting amounts as shown in Fig. 6b, we identify a gradual divergence between the ROM and the FOM that is getting increasingly evident over time. At $t = 130$, the shifting amounts $c(t)$ given by the FOM and the SR-OpInf ROM are -3.240 and -3.226 , respectively. This discrepancy likely stems from the numerical approximation (45) of the time integral of $c(t)$, which introduces accumulation error over time. Since even minor spatial misalignments can induce significant discrepancies in the scalar field $u(x, t)$ evaluated in the original frame, we attribute the primary source of prediction error to the imperfect reconstruction of

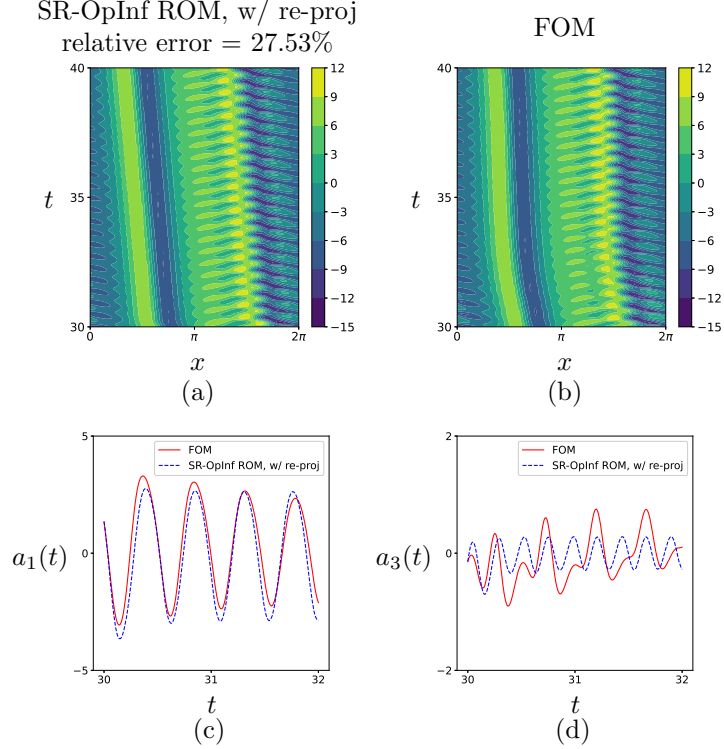


Fig. 7: Model performance on the testing dataset. Panel (a): Reconstructions of the testing snapshots from $t = 30$ to $t = 40$ given by the SR-OpInf ROM trained on re-projected dataset. Panel (b): The testing snapshots from $t = 30$ to $t = 40$. Panel (c)–(d): Amplitudes of the first $a_1(t)$ and the third $a_3(t)$ POD modes during $t \in [30, 32]$, comparing the FOM (—) and the ROM prediction (---).

shifting amount. It is also worth emphasizing that $\dot{c}(t)$ is neither constant nor sign-definite as suggested in the FOM snapshots (e.g., Fig. 2). This is due to the oscillatory beating behavior and the need to continuously align the solution with the reference template.

In addition to reconstructing the training data, we assess the generalization performance of the SR-OpInf ROM by testing its performance of reconstructing a separate set of snapshots collected during the transient stage from $t = 30$ to $t = 40$. Fig. 7 shows the resulting snapshots. Compared to the training scenario, the testing error increases significantly to 27.29%. Despite the change in initial condition, we notice that the SR-OpInf ROM trajectory still converges to the same periodic beating-wave solution seen in the training data, suggesting that the model struggles to recognize or reproduce the transient dynamics accurately. This behavior is expected as our SR-OpInf ROM trained solely on periodic data effectively replicates the behavior of a SR-Galerkin ROM, which is known to perform poorly in capturing transients not present in the

training set. To further analyze this limitation, we examine the evolution of the first and third POD mode amplitudes during the early testing interval $t \in [30, 32]$, see Fig. 7c–7d. While the FOM exhibits non-periodic dynamics, the SR-OpInf ROM rapidly returns to the previously learned periodic orbit, showing little sensitivity to the new initial condition. Although we expect that the transient can eventually be captured by the ROM with an increased number of POD modes, this comes with a painful trade-off between accuracy and computational cost and is beyond the scope of our current work. Instead, a more systematic and pragmatic approach is to seek an oblique Petrov–Galerkin projection non-intrusively [34], which has shown promise in improving the reconstruction of transients, especially when standard POD-based orthogonal projections fall short. We are currently exploring the possibility of incorporating this recently proposed approach into our framework to enhance the accuracy of the SR-OpInf ROM in capturing a broader range of dynamics without requiring an excessive number of modes.

5 Conclusion

In this paper, we introduced a novel non-intrusive reduced-order modeling (ROM) framework for approximating the dynamics of shift-equivariant systems commonly encountered in advection-dominated problems with spatially shifting solutions. Our approach builds upon the standard operator inference (OpInf) algorithm, which constructs ROMs directly from data without requiring access to the underlying governing equations. To handle symmetry, we incorporate symmetry-reduction techniques, including template fitting and the reconstruction equation, to track and eliminate spatial translations in the solution. The resulting symmetry-reduced operator inference (SR-OpInf) ROM mirrors its intrusive counterpart, the symmetry-reduced Galerkin (SR-Galerkin) ROM, but is entirely data-driven. The core of the model is a reduced-order system that governs the evolution of a profile spatially aligned to a reference template. In addition to standard polynomial terms that approximate the full-order dynamics, the model includes an advection correction term, whose speed is determined as a rational algebraic function of the reduced variable via the reconstruction equation. This allows the SR-OpInf ROM to not only track the evolution of the spatial profile but also predict the instantaneous shifting speed, enabling full reconstruction of the original, shifting field.

Training the SR-OpInf model involves minimizing the combined discrepancy in both the polynomial dynamics and the symmetry-reducing advection term. As with standard OpInf models, the resulting minimization problem is a least-squares problem, which is convex and thus has a unique global minimizer. We also present a generalization of the re-projection method presented in [28], which ensures that the learned SR-OpInf operators converge to those obtained via Galerkin projection in the SR-Galerkin ROM.

We apply this framework to the Kuramoto–Sivashinsky equation, a one-dimensional PDE which exhibits traveling beating-wave solutions. Our results show that the SR-OpInf ROM achieves an order-of-magnitude dimensionality reduction while maintaining high-fidelity reconstructions of both training and testing data.

Moreover, when trained on re-projected data, the SR-OpInf ROM yields predictions that exactly match those of the SR-Galerkin ROM constructed on the same basis—validating the effectiveness of our re-projection strategy and showing that a non-intrusive model can emulate the behavior of its intrusive counterpart.

A limitation of our approach is that it can track only a single traveling wave: if there are multiple coherent structures traveling at different speeds, our method cannot “freeze” all structures simultaneously. Some approaches have been considered for such systems [14], and one could imagine applying similar methods in the fully data-driven setting.

Another direction for future research is to combine our symmetry reduction approach with non-intrusive methods for constructing oblique projection operators [34]. These methods have the potential to overcome the limitations of orthogonal projection inherent in POD-based ROMs and enhance the model’s ability to capture transient dynamics.

Supplementary information. Not applicable.

Acknowledgements. Not applicable.

Declarations

Funding

We gratefully acknowledge support from the Air Force Office of Scientific Research, award FA9550-19-1-0005.

Conflict of Interest

The authors declared that they have no conflict of interest.

Ethics approval and consent to participate

Not applicable.

Consent for publication

Not applicable.

Data availability

All datasets and figures supporting the findings of this article are available from the corresponding author upon reasonable request.

Materials availability

Not applicable.

Code availability

The code used in this study is available at our public GitHub repository: <https://github.com/Yu-Shuai-PU/SROpInf>.

Author Contributions

Both authors contributed to the study conception. Algorithm design, material preparation, data collection and analysis were performed by Yu Shuai. The first draft of the manuscript was written by Yu Shuai and both authors worked on revisions to the manuscript. Both authors read and approved the final manuscript.

References

- [1] Wedin, H., Kerswell, R.R.: Exact coherent structures in pipe flow: travelling wave solutions. *J. Fluid Mech.* **508**, 333–371 (2004) <https://doi.org/10.1017/S0022112004009346>
- [2] Avila, M., Mellibovsky, F., Roland, N., Hof, B.: Streamwise-localized solutions at the onset of turbulence in pipe flow. *Phys. Rev. Lett.* **110**, 224502 (2013) <https://doi.org/10.1103/PhysRevLett.110.224502>
- [3] Willis, A.P., Cvitanović, P., Avila, M.: Revealing the state space of turbulent pipe flow by symmetry reduction. *J. Fluid Mech.* **721**, 514–540 (2013) <https://doi.org/10.1017/jfm.2013.75>
- [4] Willis, A.P., Short, K.Y., Cvitanović, P.: Symmetry reduction in high dimensions, illustrated in a turbulent pipe. *Phys. Rev. E* **93**, 022204 (2016) <https://doi.org/10.1103/PhysRevE.93.022204>
- [5] Ritter, P., Mellibovsky, F., Avila, M.: Emergence of spatio-temporal dynamics from exact coherent solutions in pipe flow. *New J. Phys.* **18**(8), 083031 (2016) <https://doi.org/10.1088/1367-2630/18/8/083031>
- [6] Budanur, N.B., Short, K.Y., Farazmand, M., Willis, A.P., Cvitanović, P.: Relative periodic orbits form the backbone of turbulent pipe flow. *J. Fluid Mech.* **833**, 274–301 (2017) <https://doi.org/10.1017/jfm.2017.699>
- [7] Sirovich, L.: Turbulence and the dynamics of coherent structures part i: coherent structures. *Q. Appl. Math.* **45**(3), 561–571 (1987) <http://www.jstor.org/stable/43637457>
- [8] Berkooz, G., Holmes, P., Lumley, J.L.: The proper orthogonal decomposition in the analysis of turbulent flows. *Annu. Rev. Fluid Mech.* **25**, 539–575 (1993) <https://doi.org/10.1146/annurev.fl.25.010193.002543>
- [9] Greif, C., Urban, K.: Decay of the Kolmogorov N-width for wave problems. *Appl. Math. Lett.* **96**, 216–222 (2019) <https://doi.org/10.1016/j.aml.2019.05.013>

- [10] Kirby, M., Armbruster, D.: Reconstructing phase space from PDE simulations. *Z. angew. Math. Phys.* **43**, 999–1022 (1992) <https://doi.org/10.1007/BF00916425>
- [11] Rowley, C.W., Marsden, J.E.: Reconstruction equations and the Karhunen-loève expansion for systems with symmetry. *Physica D* **142**, 1–19 (2000) [https://doi.org/10.1016/S0167-2789\(00\)00042-7](https://doi.org/10.1016/S0167-2789(00)00042-7)
- [12] Rowley, C.W., Kevrekidis, I.G., Marsden, J.E., Lust, K.: Reduction and reconstruction for self-similar dynamical systems. *Nonlinearity* **16**(4), 1257 (2003) <https://doi.org/10.1088/0951-7715/16/4/304>
- [13] Budanur, N.B., Cvitanović, P., Davidchack, R.L., Siminos, E.: Reduction of SO(2) symmetry for spatially extended dynamical systems. *Phys. Rev. Lett.* **114**, 084102 (2015) <https://doi.org/10.1103/PhysRevLett.114.084102>
- [14] Reiss, J., Schulze, P., Sesterhenn, J., Mehrmann, V.: The shifted proper orthogonal decomposition: A mode decomposition for multiple transport phenomena. *SIAM J. Sci. Comput.* **40**(3), 1322–1344 (2018) <https://doi.org/10.1137/17M1140571>
- [15] Mendible, A., Brunton, S.L., Aravkin, A.Y., Lowrie, W., Nathan Kutz, J.: Dimensionality reduction and reduced-order modeling for traveling wave physics. *Theor. Comput. Fluid Dyn.* **34**, 385–400 (2020) <https://doi.org/10.1007/s00162-020-00529-9>
- [16] Peherstorfer, B.: Model reduction for transport-dominated problems via online adaptive bases and adaptive sampling. *SIAM J. Sci. Comput.* **42**(5), 2803–2836 (2020) <https://doi.org/10.1137/19M1257275>
- [17] Rowley, C.W., Mezić, I., Bagheri, S., Schlatter, P., Henningson, D.S.: Spectral analysis of nonlinear flows. *J. Fluid. Mech.* **641**, 115–127 (2009) <https://doi.org/10.1017/S0022112009992059>
- [18] Schmid, P.J.: Dynamic mode decomposition of numerical and experimental data. *J. Fluid Mech.* **656**, 5–28 (2010) <https://doi.org/10.1017/S0022112010001217>
- [19] Tu, J.H., Rowley, C.W., Luchtenburg, D.M., Brunton, S.L., Nathan Kutz, J.: On dynamic mode decomposition: Theory and applications. *J. Comput. Dyn.* **1**(2), 391–421 (2014) <https://doi.org/10.3934/jcd.2014.1.391>
- [20] Peherstorfer, B., Willcox, K.: Data-driven operator inference for nonintrusive projection-based model reduction. *Comput. Methods Appl. Mech. Eng.* **306**, 196–215 (2016) <https://doi.org/10.1016/j.cma.2016.03.025>
- [21] Qian, E., Kramer, B., Peherstorfer, B., Willcox, K.: Lift & Learn: Physics-informed machine learning for large-scale nonlinear dynamical systems. *Physica D* **406**, 132401 (2020) <https://doi.org/10.1016/j.physd.2020.132401>

- [22] Kramer, B., Peherstorfer, B., Willcox, K.E.: Learning nonlinear reduced models from data with operator inference. *Annu. Rev. Fluid Mech.* **56**, 521–548 (2024) <https://doi.org/10.1146/annurev-fluid-121021-025220>
- [23] Baddoo, P.J., Herrmann, B., McKeon, B.J., Nathan Kutz, J., Brunton, S.L.: Physics-informed dynamic mode decomposition. *Proc. R. Soc. A* **479**(2271), 20220576 (2023) <https://doi.org/10.1098/rspa.2022.0576>
- [24] Sesterhenn, J., Shahirpour, A.: A characteristic dynamic mode decomposition. *Theor. Comput. Fluid Dyn.* **33**, 281–305 (2019) <https://doi.org/10.1007/s00162-019-00494-y>
- [25] Marensi, E., Yalniz, G., Hof, B., Budanur, N.B.: Symmetry-reduced dynamic mode decomposition of near-wall turbulence. *J. Fluid Mech.* **954**, 10 (2023) <https://doi.org/10.1017/jfm.2022.1001>
- [26] Engel, M., Ashtari, O., Schneider, T.M., Linkmann, M.: Search for unstable relative periodic orbits in channel flow using symmetry-reduced dynamic mode decomposition. *J. Fluid. Mech.* **1013**, 45 (2025) <https://doi.org/10.1017/jfm.2025.10255>
- [27] Issan, O., Kramer, B.: Predicting solar wind streams from the inner-heliosphere to Earth via shifted operator inference. *J. Comput. Phys.* **473**, 111689 (2023) <https://doi.org/10.1016/j.jcp.2022.111689>
- [28] Peherstorfer, B.: Sampling low-dimensional markovian dynamics for preasymptotically recovering reduced models from data with operator inference. *SIAM J. Sci. Comput.* **42**(5), 3489–3515 (2020) <https://doi.org/10.1137/19M1292448>
- [29] Philip, H., Lumley, J.L., Berkooz, G., Rowley, C.W.: *Turbulence, Coherent Structures, Dynamical Systems And Symmetry*, 2nd edn. Cambridge University Press, Cambridge (2012)
- [30] Kevrekidis, I.G., Nicolaenko, B., Scovel, J.C.: Back in the saddle again: A computer assisted study of the Kuramoto–Sivashinsky equation. *SIAM J. Appl. Math.* **50**(3), 760–790 (1990) <https://doi.org/10.1137/0150045>
- [31] Zang, T., Hussaini, M.: Numerical experiments on subcritical transition mechanisms. *AIAA 23rd Aerospace Sciences Meeting*, 1985–0296 <https://doi.org/10.2514/6.1985-296>
- [32] Peyret, R.: *Spectral Methods for Incompressible Viscous Flow*. Springer, New York (2002)
- [33] Mathews, K.D., Fink, J.H.: *Numerical Methods Using MATLAB*, 3rd edn. Prentice Hall, Upper Saddle River (1998)

- [34] Padovan, A., Vollmer, B., Bodony, D.J.: Data-driven model reduction via non-intrusive optimization of projection operators and reduced-order dynamics. *SIAM J. Appl. Dyn. Syst.* **23**(4), 3052–3076 (2024) <https://doi.org/10.1137/24M1628414>